Spectroscopic Properties and Potential Energy Surfaces of Electronic States of $SbCl_2$, $SbBr_2$, $SbCl_2^+$ and $SbBr_2^+$

K. Balasubramanian* and Lida Latifzadeh-Masoudipour

Department of Chemistry and Biochemistry, Arizona Sate University, Tempe, Arizona 85287-1604

Received: July 8, 1998; In Final Form: January 8, 1999

Spectroscopic properties and bending potential energy surfaces of $^2B_1$, $^2A_1$, $^2A_2$, $^2A_2(^2\Pi_g)$, $^4A_2(^4\Pi_g)$, $^4B_1(^4\Sigma_g^-)$ and $^2B_2$ electronic states of $SbCl_2$ and $SbBr_2$, and three low-lying electronic states of $SbCl_2^+$ and $SbBr_2^+$, ($^1A_1$, $^3B_1$, $^1B_1$), have been studied with complete active space self-consistent field (CASSCF) followed by multireference singles and doubles configuration interaction (MRSDCI) methods that included nearly 2 million configurations. The bond dissociation and adiabatic ionization energies of $SbCl_2$, $SbBr_2$, SbCl, and SbBr have been computed. The computed properties of these species are extensively compared with other group V dihalides.

I. Introduction

Halogen etching of III−V semiconductors is of prime importance in the fabrication of fast III−V microelectronic devices.[1−5] Among the III−V semiconductors, the InSb semiconductor finds significant application as a detector in the FT-IR spectrometer for near-infrared region.[1] Typically, halogen etching of InSb semiconductor generates SbX_2[6] as one of the products. Thus the spectroscopic and electronic properties of the dihalides of Sb can be potentially useful in the evaluation of the manufacturing process of these semiconductors. Moreover, such evaluations require accurate information on the various thermochemical enthalpies and bond energies for the processes involved in the etching of semiconductors. For example, during the etching of GaAs by chlorine, AsCl, $AsCl_2$, and $AsCl_3$ are all obtained, among which the $AsCl_2$ radical is a major product monitoring the etching rate.[7]

The ionization energy of $SbCl_2$ and $SbBr_2$ can give useful information for the local impedance variations of plasma reactor during the dry-halogen etching process.[8] The bond dissociation energies of these antimony halides have an important impact in transferring Sb away from the semiconductor surface during the halogen-etching process.

Organometallic compounds containing antimony have been synthesized and characterized by a few workers.[9−12] Edwards and co-workers[9] have reported the bond length of SbCl in the range of 2.445−2.66 Å and the ClSbCl bond angles near 91.46° for dimeric antimony complexes capturing dimethylamine as a neutral donor. Wiley et al.[10] have obtained the crystal structure of antimony organometallic compound with 1,4,7-trimethyl-1,4,7 triazacyclononane as a ligand. The central cation of this organometallic compound is $SbCl_2^+$ in which the Sb−Cl bond length is reduced to 2.466 Å compared to a value of 2.596 Å in the neutral metal derivatives.[12]

Spectroscopic investigations and calculations have been carried out on several group V difluorides[13−17] such as PF_2,[13−14,17] PCl_2, PBr_2,[20,21] AsF_2,[15] and BiF_2.[16] It has been observed that the ground electronic states of both PF_2 and AsF_2 are X^2B_1 states. The structural parameters of the ground state of PF_2 have been deduced from the microwave spectrum[13] as P−F = 1.5792 Å and FPF = 98.48°. The geometry parameters[24] of AsF_2 in the X^2B_1 ground state are As−F = 1.74 Å and FAsF = 96°. Bramwell et al.[21] have obtained the electronic spectrum of PCl_2. The observed spectrum consists of a series of structureless bands between 360 and 800 nm region. Brum and Hudgens[17] have observed two Rydberg states of the PCl_2 radical using resonance-enhanced multiphoton ionization (REMPI) spectroscopy. These authors have also carried out ab initio G2 computations of this radical. Berkowitz et al. [18] have studied PF_2 radical with photoionization mass sepctroscopy, which yielded the adiabatic ionization energy of PF_2 to be 8.847 eV.

The related PBr_2 radical was observed by Andrews and Frederick[20] by simultaneous condensation of PBr_3 in an Ar matrix. The radical has been also generated in the flash photolysis of PBr_3 using 193 and 248 nm laser.[21] Bramewell et al.[21] have observed a broad and structureless emission system in the 193 nm attributed to the $A^2A_1-X^2B_1$ system by these authors. A remarkable feature of this system is that the lifetime of the A state was found to be quite long (21 μs). The emission systems in the 248 nm laser photolysis have not been fully characterized. Zhao and Setser[22] have studied the reactive quenching of an excited electronic state of the related diatomic PF by molecules such as F_2, Cl_2, Br_2, etc.

Although theoretical studies have been made on other related group V halides,[23−25] there are no theoretical studies on $SbCl_2$, $SbBr_2$, $SbCl_2^+$, and $SbBr_2^+$. Related theoretical studies have been done on PH_2^+ by Schaefer and co-workers[36] as well as by Balasubramanian[37] on both the ground (X^1A_1) and excited triplet (a^3B_1) and singlet (A^1B_1) electronic states. Similar studies have been done on the isovalence electronic NH_2^+ by Schaefer and co-workers.[38] Ab initio computations have been made on the low-lying electronic states of the lighter NF_2 radical[39] as well as PCl_n.[40] Related group IV dihydrides as well as heavier group V dihydrides have also been considered before.[41] There are also other theoretical studies on the diatomic group V halides such as SbF and SbI.[42,43] For a complete review of the work done on these species, see Balasubramanian's books.[35]

In the current study, we have used high-level ab initio calculations for $SbCl_2$ and $SbBr_2$ to study X^2B_1, $^2A_1$, $^2A_2$, $^2A_2(^2\Pi_g)$, $^4A_2(^4\Pi_g)$, $^4B_1(^4\Sigma_g^-)$, and $^2B_2$ electronic states as well as the X^1A_1, $^3B_1$, and $^1B_1$ electronic states of $SbCl_2^+$ and $SbBr_2^+$ employing the CASSCF/MRSDCI techniques that included

10.1021/jp982921q CCC: $18.00
Published on Web 04/06/1999

nearly 2 million configurations. Geometries, energy separations (T_e), electric dipole moments (μ_e), bond dissociation energies (D_e), and adiabatic ionization energies have been computed. The singlet(X^1A_1)−triplet($^3B_1$) and the singlet(X^1A_1)−singlet($^1B_1$) energy separations of the positive ion have been determined. In addition, the ground state properties and the dissociation energies of the corresponding diatomic species have been computed.

II. Method of Theoretical Computations

All the calculations were performed employing relativistic effective core potentials (RECPs). The outer $5s^25p^3$ shells for Sb, $3s^23p^5$ shells for Cl, and $4s^24p^5$ shells for Br were kept in the valence space, replacing the remaining core electrons by RECPs.[26,27] Valence Gaussian (3s3p) basis sets together with the RECPs for Sb[26] were augmented with two 3d polarization functions having $\alpha_{d1} = 0.130\ 50$ and $\alpha_{d2} = 0.050\ 34$. The (4s4p) valence Gaussian basis set for chlorine was contracted to (3s3p) by contracting the first two large exponent functions. The resulting basis set was augmented with two sets of 3d polarization functions with $\alpha_{d1} = 0.220$ and $\alpha_{d2} = 0.797$.[28] For Br, the 3s3p valence Gaussian basis set was augmented with $\alpha_{d1} = 0.548$ and $\alpha_{d2} = 0.1162$.[28] Consequently, our final valence Gaussian basis sets were of (3s3p2d) quality for all atoms.

In order to test the effects of 4d-shell electron correlation effects especially on the bond dissociation energies, we carried out computatrions that included the $4d^{10}$ shells in the valence space. Consequently, we invoked the RECPs that retained the $4d^{10}5s^25p^3$ shells of the Sb atom in the valence space replacing the remaining electrons in the core by RECPs. The corresponding valence Gaussian basis sets were taken from ref 26.

We started with the CASSCF computations, which were followed by the higher order MRSDCI computations using the orbitals generated by the CASSCF method. The 3s electrons of Cl and 4s electrons of Br were maintained inactive in the CASSCF calculations in that excitations were not allowed, but these orbitals were relaxed as a function of their geometries. Therefore, the CASSCF active space consisted of four a_1, three b_2, two b_1, and one a_2 orbitals for each species. All the valence electrons except the halogen s electrons (and thus a total of 15 electrons) were distributed in all possible ways among these orbitals. The MRSDCI method included excitations from the 3s electrons of Cl and the 4s electrons of the Br atoms. All electronic configurations with coefficients ≥ 0.09 were chosen as reference configuration at the MRSDCI stage.

We computed the vibrational frequencies of the halides and their positive ions using the unrestricted Møller−Plesset second-order perturbation theory (UMP2) as well as unrestricted density function theory (DFT) employing B3LYP potentials. The vibrational frequencies were computed using the second energy gradients.

The geometries and energy separations of all electronic states were fully optimized at both the CASSCF and MRSDCI levels of theory. The dissociation energies of SbCl−Cl and SbBr−Br bonds were obtained by carrying out supermolecular computations on $SbCl_2$ and $SbBr_2$ by setting one of the Sb−Cl bond lengths to 2.374 Å (r_e of SbCl in the $^3\Sigma^-$ ground state) and the other Sb−Cl distance to 10 Å for a linear geometry of the X^2B_1 state. For $SbBr_2$, one Sb−Br bond length was set to 2.538 Å (r_e of SbBr in the $^3\Sigma^-$ ground state) and the other Sb−Br bond to 10 Å. The CASSCF/full second-order CI (SOCI) computations were performed on both SbBr and SbCl species at both the equilibrium geometry and the $^4S + {}^2P$ dissociation limits. Spin−orbit effects were applied to correct the dissociation energies. The effect of 4d electron correaltions was computed by carring out CASSCF/MRSDCI computations on $SbCl_2$, $SbBr_2$, and the corresponding diatomics by allowing single and double excitations from the 4d shells. All the calculations were performed using Balasubramanian's[29] modified version of ALCHEMY codes[30] to include the relativistic RECPs.

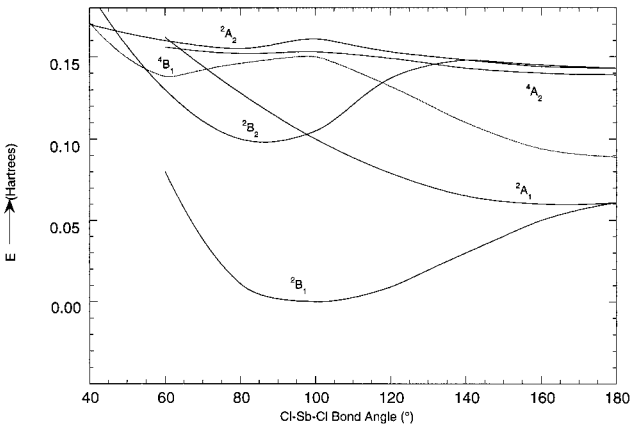

Figure 1. Bending potential energy surfaces for the electronic states of $SbCl_2$.

III. Results and Discussions

A. $SbCl_2$. The bending potential energy surfaces of SbCl2 with Sb−Cl bond length optimized for each ClSbCl bond angle (θ) are shown in Figure 1. As evidenced from Figure 1, the ground state of $SbCl_2$ is the X^2B_1 state in analogy with the other group V dihalides, while the first excited state of $SbCl_2$ is the $^2A_1$(I) state which correlates with the same linear limit as the X^2B_1 state (Figure 1). However, in contrast to phosphorus dihalides such as PBr_2[25], this state does not exhibit a bent minimum and becomes linear. This is primarily because the bending potential energy surface is quite shallow and forms only a linear minimum for the heavier halogen atoms. The first excited bent electronic state of $SbCl_2$ exhibiting a bent minimum is the $^2B_2$(I) state with an energy separation of 2.46 eV. The crossing of the bending potential energy surfaces of the $^2B_2$(I) and $^2A_1$(I) states in Figure 1 suggests a channel for the conversion between these two states through spin−orbit coupling. Furthermore, the two states would be mixed in the region of crossing as the $^2B_2$(I) state with an open-shell spin of β could interact with the $^2A_1$(I) state with an open shell spin of α as they both correlate into the same E representation in the $C_{2v}{}^2$ double group.

The $^4B_1$ state of $SbCl_2$ exhibits a very acute bent minimum near 57.2° with long Sb−Cl bond lengths of 2.709 Å and somewhat short Cl−Cl bond distance of 2.59 Å. This suggests that this state could be decribed as a loose complex of Sb−Cl_2. As seen from Figure 1, this state exhibits a lower linear minimum, which correlates into $^4\Sigma_g^-$. It should be noted that the Sb−Cl bond distances become significantly shorter (2.456 Å) for the linear state. The $^4A_2$ state exhibits a bent minimum at 85°. As seen from Figure 1, a shallow potential minimum is found for the $^2A_2$ state near 79° and the same curve exhibits a linear minimum attributed to $^2\Pi_g$ subsequent to a barrier in the potential energy surface.

The actual equilibrium geometries (r_e, θ_e), energy separations (T_e), and the dipole moments (μ_e) of nine electronic states of $SbCl_2$ at their equilibrium geometries are shown in Table 1 as obtained using the MRSDCI level of theory. The r_e(Sb−Cl) = 2.374 Å and θ_e(ClSbCl) = 98° computed here for the ground state of $SbCl_2$ compare with the values reported by Edwards

TABLE 1: Geometries and Energies of $SbCl_2$ and $SbCl_2^+$ at the CASSCF/MRSDCI Level

species	state	r_e (Å)	θ_e (deg)	T_e (eV)	μ_e (D)[a]
$SbCl_2$	X^2B_1	2.374	98.0	0	0.730
	$^2A_1(I)$	2.485	168.7	1.55 (1.52)[b]	0.210
	$^2B_2(I)$	2.452	82.4	2.46 (2.38)[b]	1.370
	$^4B_1(^4\Sigma_g^-)$	2.456	180	2.40 (2.42)[b]	
	$^4B_1$	2.709	57.2	2.94 (2.67)[b]	1.053
	$^4A_2(^4\Pi_g)$	2.709	180	3.62 (3.55)[b]	
	$^2A_2(^2\Pi_g)$	2.745	180	3.81 (3.65)[b]	
	$^2A_2$	2.568	78.8	4.24 (4.16)[b]	0.193
	$^4A_2$	2.554	84.9	4.24 (4.17)[b]	0.852
$SbCl_2^+$	$^1A_1$	2.279	99.8	8.25 (8.25)[b]	
	$^3B_1$	2.308	118.9	10.64 (10.66)[b]	
	$^1B_1$	2.419	105.6	11.06 (10.98)[b]	

[a] The positive polarity of dipole moment means Sb^+Cl^-. [b] Numbers in the parentheses include Davidson correction.

TABLE 2: Mulliken Population for $SbCl_2$ and $SbCl_2^+$ (Gross Populations)[a]

species	state	Sb	2Cl[b]	Sb(s)	Sb(p)	Sb(d)	2Cl(s)	2Cl(p)
$SbCl_2$	X^2B_1	4.06	14.94	1.84	2.05	0.165	3.96	10.75
	$^2A_1(I)$	4.09	14.91	1.87	1.87	0.350	3.95	10.75
	$^2B_2(I)$	4.18	14.82	1.87	2.06	0.249	3.95	10.67
	$^4B_1(^4\Sigma_g^-)$	4.32	14.68	1.60	2.50	0.227	3.96	10.50
	$^4B_1$	4.50	14.50	1.93	2.44	0.123	3.96	10.33
	$^4A_2(^4\Pi_g)$	4.60	14.40	1.94	2.51	0.153	3.95	10.27
	$^2A_2$	4.61	14.39	1.92	2.59	0.096	3.96	10.22
	$^2A_2(^2\Pi_g)$	4.59	14.41	1.94	2.50	0.156	3.95	10.28
	$^4A_2$	4.45	14.55	1.74	2.52	0.187	3.96	10.38
$SbCl_2^+$	$^1A_1$	3.41	14.59	1.81	1.45	0.154	3.95	10.37
	$^3B_1$	3.58	14.42	1.51	1.92	0.155	3.96	10.17
	$^1B_1$	3.79	14.21	1.83	1.89	0.076	3.96	10.00

[a] The Cl(d) populations for both Cl's are between 0.082 and 0.284. [b] Populations for both Cl atoms.

and co-workers,[9] namely, SbCl bond length in the range of 2.445−2.66 Å and the ClSbCl bond angles near 91.46° for dimeric antimony complexes capturing dimethylamine as a neutral donor.[10]

Analogous to other group V dihalides such as SbF_2, AsF_2, etc., as seen from Table 1, the $^2B_2(I)$ electronic state of $SbCl_2$ possesses the largest dipole moment. The ground state of dipole moment of $SbCl_2$ (0.730 D) with Sb^+Cl^- polarity is considerably smaller than the corresponding value for SbF_2 (1.24 D) but larger than PF_2 (0.57 D).[25] The larger value of the dipole moment of $SbCl_2$ compared to PF_2 is consistent with the decreased electronegativity of Sb compared to P, but the larger dipole moment of SbF_2 is consistent with the greater electronegativity of F compared to Cl.

The stepwise bond dissociation energy of $SbCl_2$ is of considerable interest as this value could provide important information on the thermochemistry of the processes associated with the halogen etching. We employed the MRSDCI method and a full CI estimate to the MRSDCI using Davidson's correction, which we denote as the MRSDCI+Q result.

We computed the D_e of the diatomic SbCl using the full second-order CI(SOCI). All 12 electrons of SbCl were distributed in all possible ways with respect to zeroth-order, first and second-order excitations. The geometry of SbCl in the $X^3\Sigma^-$ state was optimized at the SOCI level, yielding a value of 2.403 Å for the Sb−Cl bond length. Although there is no experimental r_e value for the $X^3\Sigma^-(0^+)$ ground state of SbCl,[33] on the basis of the experimental r_e values for the ground states of SbF, SnF, and SnCl species, an estimate of 2.38−2.40 Å is obtained, which is good agreement with our computed result. The dissociation energy of SbCl was obtained as a supermolecular computation by setting the Sb−Cl bond distance to 8 Å for the $^3\Sigma^-$ state. Larger distances up to 20 Å were also considred and made no difference whatsoever in the D_e values. The SOCI and SOCI + Q (includes quadruple corrections) yielded the D_e values of 2.61 and 2.60 eV, respectively. The spin−orbit splitting of the $X^3\Sigma^-$ state is known[33] to be 816 cm^{-1}. Using this value and the atomic spin−orbit correction for the $^4S_{3/2}$ of the antimony atom, we estimate the spin−orbit correction to lower the D_e of SbCl by 0.4−0.5 eV. The 4d electron correlation effects were computed. The D_e increases by only 0.06 eV due to 4d electron correlation effects and by 0.08 eV when quadruple cluster corrections are included. Consequently, the destabilization due to spin−orbit coupling is more than the d electron correlation effects. However, improvement in the basis set and further inclusion of electron correlation effects would increase the D_e by up to 0.2 eV. Thus we predict the D_e of SbCl as 2.5 eV. While there are no experimental D_e values on SbCl, our comparable theoretical technique yielded $D_e = 3.98$ eV for SbF consistent with a D_0 value of 4.18 eV reported by Yoo and co-workers.[16] Note that the zero-point correction for the SbCl diatomic is 187.5 cm^{-1}.

The atomization energy of $SbCl_2 \rightarrow Sb(^4S) + 2Cl(^2P)$ process was computed by setting both Sb−Cl bond lengths to 10 Å and ClSbCl = 180° for the $^2B_1$ state. The total atomization energy thus computed is 5.24 eV (5.35 eV) at MRSDCI (MRSDCI + Q) level. From these results the first stepwise bond dissociation energy of ClSb−Cl corresponding to the $SbCl_2(^2B_1) \rightarrow SbCl(^3\Sigma^-) + Cl(^2P)$ process is inferred as 2.75 eV. The 4d electron correlation effect on the first stepwise bond energy is computed as 0.03 eV at the MRSDCI level and 0.00 eV at the MRSDCI+Q level. The spin−orbit splitting of atomic Cl is rather small (881 cm^{-1}) and thus the spin−orbit stabilization of the Cl atom's $^2P_{3/2}$ state relative to the ^2P state is only 0.04 eV. The spin−orbit contributions to $SbCl_2$ (0.05 eV) and SbCl (0.1 eV) are comparable except that the contribution to $SbCl_2$ is estimated to be smaller than SbCl. Consequently, the bond dissociation energy should be decreased by 0.1 eV due to spin−orbit coupling. Consequently, the increase in the dissociation energy due to the 4d correlation effects (0.03 eV) is smaller than the decrease in the D_e due to spin−orbit coupling (0.1 eV) and the net result is that the first bond dissociation energy of $SbCl_2$ becomes 2.58 eV with d correlation and spin−orbit corrections.

The vibrational frequencies are computed at the UMP2 level as 367.7 cm^{-1} for the A_1 symmetric stretch, 354.8 cm^{-1} for the B_2 asymmetric stretch and 127.4 cm^{-1} for the A_1 symmetric bending mode for the $^2B_1$ ground state. The UB3LYP vibrational frequencies for the same state are uniformly lower. The corresponding B3LYP values are 350.2 cm^{-1} for the A_1 symmetric stretch, 335.3 cm^{-1} for the B_2 asymmetric stretch, and 117.4 cm^{-1} for the A_1 symmetric bending mode for the $^2B_1$ ground state.

Table 2 shows the gross Mulliken populations of different electronic states of $SbCl_2$ and $SbCl_2^+$. The antimony population in the X^2B_1 ground state of $SbCl_2$ is 4.06 which is further divided into $5s^{1.84}5p^{2.05}5d^{0.165}$, while the combined Cl populations is 14.94. Evidently, there is significant electron transfer (0.94) from Sb to Cl consistent with the Sb^+Cl^- polarity of the bonds and the dipole moment of $SbCl_2$. The SbF_2 ground state has a Sb population of 3.67, divided into $5s^{1.76}5p^{1.76}5d^{0.148}$, and the combined populations of the two Fs is 15.33. Consequently, the extent of electron transfer from Sb is larger for SbF_2 (1.33) compared to $SbCl_2$ (0.94) consistent with the larger electronegativity of F compared to Cl. The Sb(p) populations in some of the excited states of $SbCl_2$ are considerably higher compared

TABLE 3: Leading Configuration for $SbCl_2$ and $SbCl_2^+$, $SbBr_2$, and $SbBr_2^+$

state	coeff		$4a_1$	$5a_1$	$3b_2$	$4b_2$	$2b_1$	$1a_2$
	$SbCl_2$	$SbBr_2$						
X^2B_1	−0.980	−0.975	2	0	2	0	1	2
$^2A_1(I)$	−0.969	0.961	2	1	2	0	0	2
$^4B_1(^4\Sigma_g^-)$	0.981	−0.977	1	1	2	0	1	2
$^2B_2(I)$	0.971	−0.961	2	0	2	1	0	2
$^4B_1$	0.970	0.964	2	0	1	1	1	2
$^4A_2(^4\Pi_g)$	0.931	−0.913	2	1	1	0	1	2
$^2A_2$	−0.932	0.935	2	0	2	0	2	1
$^2A_2(^2\Pi_g)$	0.748	0.749	2	1	1	0	1	2
	0.520	0.509	2	1	1	0	1	2
$^4A_2$	0.940		1	0	2	1	1	2
	$SbBr_2^+$	$SbBr_2^+$						
$^1A_1$	−0.965	−0.960	2	0	2	0	0	2
$^3B_1$	−0.967	0.961	1	0	2	0	1	2
$^1B_1$	0.942	−0.938	1	0	2	0	1	2

[a] All states have $1a_1^2 2a_1^2 3a_1^2 1b_1^2 2b_2^2 2b_1^2 1b_1^2$ electronic configuration.

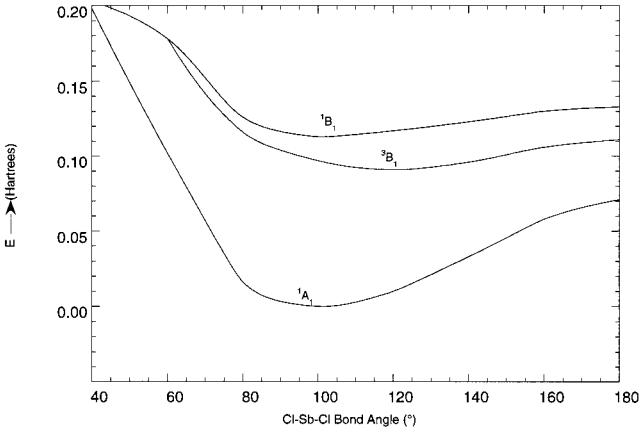

Figure 2. Bending potential energy surfaces for the electronic states of $SbCl_2^+$.

to the X^2B_1 ground state. This is attributed to the Sb(6p) Rydberg character of these excited states.

Table 3 shows the leading configurations of the electronic states of the species considered here. As seen from this table, the leading configuration of the X^2B_1 ground electronic state of $SbCl_2$ is $1a_1^2 2a_1^2 3a_1^2 4a_1^2 1b_2^2 2b_2^2 3b_2^2 1b_1^2 2b_1^1 1a_2^2$, where only the active electrons are shown. The $^2A_1(I)$ state is formed from the ground state by exciting the $2b_1$ electron into $5a_1$. The $^2A_2$ state is obtained from $^2B_1$ by promoting an electron from $1a_2$ to $2b_1$, while the $^2B_2(I)$ state is generated by transferring an electron from $2b_1$ in the X^2B_1 state to $4b_2$. The $^2B_2(II)$ state is obtained by promoting an electron from $3b_2$ to $2b_1$, while the $^4B_1$ and $^4A_2$ states are formed by promoting an electron from $3b_2$ to $4b_2$, and $4a_1$ to $4b_2$, respectively.

B. $SbCl_2^+$. Figure 2 shows the bending potential energy surfaces of the X^1A_1 and $^3B_1$ and $^1B_1$ electronic states $SbCl_2^+$. The three electronic states of $SbCl_2^+$ are similar to the other group V dihalide ions[25] and also isovalence electronic group IV dihydrides and dihalides,[41] which are known to exhibit X^1A_1 ground states and the $^3B_1$ and $^1B_1$ excited electronic states. As seen from Figure 2, the ground state of $SbCl_2^+$ is the X^1A_1 state, which arises from the removal of an electron from the singly occupied b_1 HOMO of the $SbCl_2$ neutral species. The excited states of $SbCl_2^+$ are generated by removing an electron from the highest occupied $4a_1$ orbital of the $SbCl_2$ ground state. The $^3B_1$ and $^1B_1$ excited states exhibit minima near $\theta = 106°-119°$.

The equilibrium geometries and the energy separations of three electronic states of $SbCl_2^+$ are shown in Table 1. The

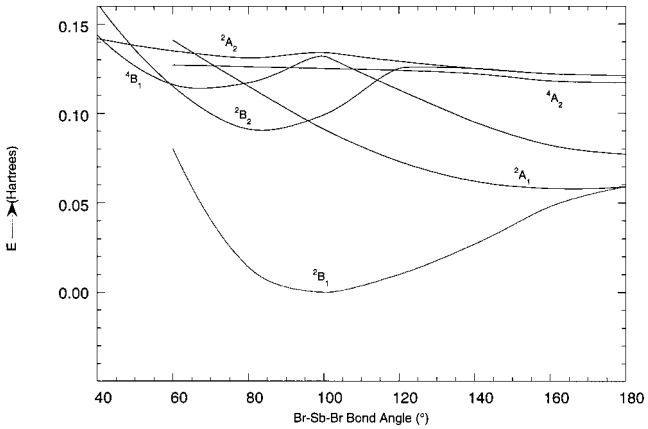

Figure 3. Bending potential energy surfaces for the electronic states of $SbBr_2$.

TABLE 4: Geometries and Energies of $SbBr_2$ and $SbBr_2^+$ at the CASSCF/MRSDCI Level

species	state	r_e (Å)	θ_e (deg)	T_e (eV)	μ_e (D)[a]
$SbBr_2$	X^2B_1	2.538	102.0	0	0.892
	$^2A_1(I)(^2\Pi_u)$	2.646	180	1.46 (1.41)[b]	
	$^2B_2(I)$	2.628	84.0	2.38 (2.29)[b]	1.29
	$^4B_1(^4\Sigma_g^-)$	2.625	180	1.82 (1.69)[b]	
	$^4B_1$	2.881	59.7	2.42 (2.27)[b]	1.03
	$^4A_2(^4\Pi_g)$	2.865	180	2.93 (2.88)[b]	
	$^2A_2$	2.679	79.4	3.60 (3.55)[b]	0.019
	$^2A_2(^2\Pi_g)$	2.915	180	3.10 (2.97)[b]	
$SbBr_2^+$	$^1A_1$	2.436	101.1	8.09 (8.08)[b]	
	$^3B_1$	2.471	120.1	10.06 (10.07)[b]	
	$^1B_1$	2.578	106.3	10.26 (10.25)[b]	

aThe positive polarity of dipole moment means Sb+Br−. [b] Numbers in the parentheses include Davidson correction.

ground state of $SbCl_2^+$ is $^1A_1$ with Sb−Cl = 2.279 Å and θ_e = 99.8°, which can be compared with the corresponding values of SbF_2^+ (Sb−F = 1.820 Å and θ_e = 96.3°).[25] The longer Sb−Cl bond lengths and larger Cl−Sb−Cl bond angle are consistent with the larger sizes of the chlorine atoms. The adiabatic ionization energy of $SbCl_2$ for the process of $SbCl_2(X^2B_1) \rightarrow SbCl_2^+(^1A_1) + e^-$ was computed as 8.25 eV at the highest level of theory. This value is remarkably close to the adiabatic ionization energy of SbF_2,[25] which was previously computed as 8.33, and 8.22 eV at the MRSDCI and MRSDCI+Q levels, respectively.

As seen from Table 1, analogous to group IV hydrides and halides, we find excited $^3B_1$ and $^1B_1$ states. The first excited $^3B_1$ state has a bent equilibrium geometry with r_e(Sb−Cl) = 2.308 Å and θ_e = 118.9°. The $^1B_1$ state, which arises from the same electronic configuration, has an MRSDCI optimized geometry of r_e(Sb−Cl) = 2.419 Å and θ_e = 105.6°. Our $^3B_1-X^1A_1$ energy separation for $SbCl_2^+$ is 2.39 eV at the MRSDCI level and 2.41 eV at the MRSDCI + Q level. This compares with the corresponding singlet−triplet and singlet−singlet energy separations of 3.91 and 4.09 eV obtained earlier for SbF_2^+ at the MRSDCI and MRSDCI + Q levels, respectively.[25] The $^1B_1-X^1A_1$ energy separation for $SbCl_2^+$ is 2.81 and 2.73 eV, respectively, at the MRSDCI and MRSDCI + Q levels. The corresponding energy separations for SbF_2^+ are 5.07 and 5.00 eV at MRSDCI and MRSDCI + Q levels, respectively.[25] The smaller energy separations for the $SbCl_2^+$ compared to SbF_2^+ are consistent with the fact that the halogen (p) orbitals change significantly in the formation of $^3B_1$ and $^1B_1$ states from X^1A_1, and it is easier to deform the chlorine (p) compared to F(p) as the former orbital is more diffuse than the latter.

TABLE 5: Mulliken Population for $SbBr_2$ and $SbBr_2^+$, (Gross Populations)[a]

species	state	Sb	2Br[b]	Sb(s)	Sb(p)	Sb(d)	2Br(s)	2Br(p)
$SbBr_2$	X^2B_1	4.19	14.81	2.00	2.17	0.0138	4.06	10.64
	$^2A_1(I)(^2\Pi_u)$	4.35	14.65	2.08	1.94	0.333	4.06	10.55
	$^2B_2(I)$	4.33	14.67	2.03	2.20	0.092	4.05	10.53
	$^4B_1(^4\Sigma_g^-)$	4.66	14.34	1.88	2.52	0.252	4.09	10.26
	$^4B_1$	4.54	14.46	2.04	2.49	0.008	4.09	10.29
	$^4A_2(^4\Pi_g)$	4.67	14.33	2.05	2.53	0.094	4.10	10.23
	$^2A_2$	4.65	14.35	2.02	2.63	0.005	4.09	10.18
	$^2A_2(^2\Pi_g)$	4.66	14.34	2.05	2.52	0.084	4.10	10.25
$SbBr_2^+$	$^1A_1$	3.67	14.33	2.03	1.66	0.025	4.09	10.16
	$^3B_1$	3.81	14.19	1.83	2.03	0.052	4.11	9.98
	$^1B_1$	3.99	14.01	2.02	1.97	0.01	4.12	9.89

[a] The Br(d) populations for both Br's are between 0.006 and 0.093. [b] Populations for both Br atoms.

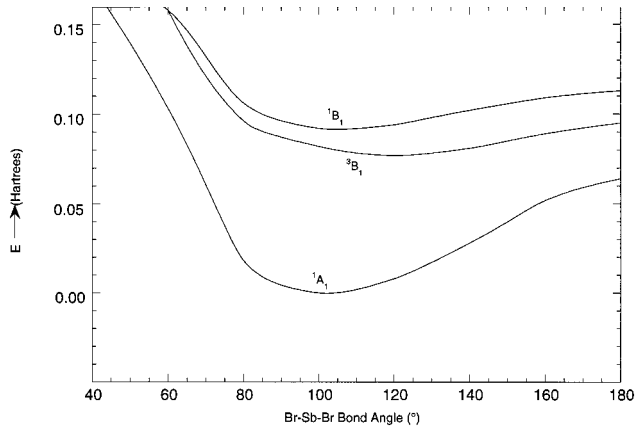

Figure 4. Bending potential energy surfaces for the electronic states of $SbBr_2^+$.

The vibrational frequencies are computed at the UMP2 level as 419.7 cm^{-1} for the A_1 symmetric stretch, 412.6 cm^{-1} for the B_2 asymmetric stretch, and 143.6 cm^{-1} for the A_1 symmetric bending mode for the $^1A_1$ ground state of $SbCl_2^+$. The UB3LYP vibrational frequencies for the same state are uniformly lower consistent with the neutral results. The corresponding B3LYP values are 400.5 cm^{-1} for the A_1 symmetric stretch, 390.9 cm^{-1} for the B_2 asymmetric stretch, and 135.5 cm^{-1} for the A_1 symmetric bending mode for the $^1A_1$ ground state.

The Mulliken populations in Table 2 reveal that the $^1A_1$ electronic state of $SbCl_2^+$ has an Sb population of 3.41 and a combined Cl population of 14.59. This suggests that 65% of the electronic charge is removed from Sb atom upon ionization of $SbCl_2$ in the X^2B_1 state. The Cl(p) populations of the $^3B_1$ and $^1B_1$ states of $SbCl_2^+$ are strikingly smaller compared to the X^1A_1 state of $SbCl_2^+$. The reductions are large (0.20 and 0.37) for the $^3B_1$ and $^1B_1$ states, consistent with the large $^3B_1-X^1A_1$ and $^1B_1-X^1A_1$ energy separations for $SbCl_2^+$ as compared to SbH_2^+.[41] The Sb(5p) populations are increased in the $^3B_1$ and $^1B_1$ states of $SbCl_2^+$ compared to the X^1A_1 state.

As seen from Table 3, the ground state of $SbCl_2^+$ is described by $1a_1^2 2a_1^2 3a_1^2 4a_1^2 1b_2^2 2b_2^2 3b_2^2 1b_1^2 1a_2^2$ configuration, while the $^3B_1$ and $^1B_1$ excited states originate from the $1a_1^2 2a_1^2 3a_1^2 4a_1^1 1b_2^2 2b_2^2 3b_2^2 1b_1^2 2b_1^1 1a_2^2$ configurations.

C. $SbBr_2$. Since there are some similarities between the bromide and chloride species, we shall restrict our discussion of the bromide species only to important points and proceed to compare different species in section IIIE. The bending potential energy surfaces of $SbBr_2$ (Sb−Br bond length optimized) for each BrSbBr bond angle (θ) are shown in Figure 3. Analogous to $SbCl_2$, as seen from Figure 3, the ground state of $SbBr_2$ is the X^2B_1 state, while the first excited state of $SbBr_2$ is the $^2A_1(I)$ (Figure 3). The first bent excited electronic state of $SbBr_2$ is the $^2B_2(I)$ state with an energy separation of 2.38 eV. Similar to $SbCl_2$, the crossing of the bending potential energy surfaces of the $^2B_2(I)$ and $^2A_1(I)$ states (Figure 3) provides a channel for the interaction between these two states through spin−orbit coupling. The $^4B_1$ state of $SbBr_2$ exhibits an acute bent minimum near 59.7° with long Sb−Br bond lengths of 2.881 Å, and a lower linear Σ_g^{4-} minimum. In contrast to $SbCl_2$, the $^4A_2$ state exhibits a very flat bending potential energy curve (Figure 3) and thus does not form a bent minimum at 85°. On the other hand, the $^2A_2$ state exhibits two minima, one at 79.4° and the other linear minimum attributed to $^2\Pi_g$.

Table 4 shows the actual equilibrium geometries (r_e, θ_e), energy separations (T_e), and the dipole moments (μ_e) of eight electronic states of $SbBr_2$. The ground state of dipole moment of $SbBr_2$ (0.892 D) with Sb^+Br^- polarity is smaller than the corresponding values for SbF_2 (1.24 D) but larger than PF_2 (0.57 D). There are many similarities between the computed spectroscopic properties of $SbBr_2$ and $SbCl_2$ as seen from Tables 1 and 4.

We computed the D_e of the diatomic SbBr using the full second-order CI(SOCI). The geometry of SbBr in the $X^3\Sigma^-$ state was optimized at the SOCI level, yielding a value of 2.566 Å for the Sb−Br bond length. The SOCI technique yielded the D_e value of 2.23 eV for SbBr. The effect of 4d electron correlation effects increases the D_e by 0.08 eV. The spin−orbit coupling reduces the D_e of SbBr by 0.17 eV, so that the spin−orbit destabilization is larger than the 4d electron correlation effects. The D_e of SbBr corrected for both 4d electron correlation effects and spin−orbit coupling is 2.1 eV. The zero-point correction for the SbBr diatomic is only 121 cm^{-1}.

The atomization energy of $SbBr_2 \rightarrow Sb(^4S) + 2Br(^2P)$ process was computed as 4.28 eV at the MRSDCI level. From these results the first stepwise bond dissociation energy of BrSb−Br corresponding to $SbBr_2(^2B_1) \rightarrow SbBr(^3\Sigma^-) + Br(^2P)$ process is inferred as 2.05 eV. The d correlation effects increase the first bond dissociation energy by 0.07 eV. The spin−orbit correction destabilizes the bond dissociation energy by 0.2 eV. Consequently, the first bond D_e, corrected for both spin−orbit and d correlation effects, is 1.9 eV.

The vibrational frequencies are computed at the UMP2 level as 238.1 cm^{-1} for the A_1 symmetric stretch, 235.0 cm^{-1} for the B_2 asymmetric stretch, and 79.8 cm^{-1} for the A_1 symmetric bending mode for the $^2B_1$ ground state of $SbBr_2$. The corresponding B3LYP values are 234.1 cm^{-1} for the A_1 symmetric stretch, 229.2 cm^{-1} for the B_2 asymmetric stretch, and 75.0 cm^{-1} for the A_1 symmetric bending mode for the $^2B_1$ ground state.

Table 5 shows the gross Mulliken populations of different electronic states of $SbBr_2$ and $SbBr_2^+$. In comparing Tables 2 and 5, it is noted that the antimony populations in most of the electronic states of $SbBr_2$ are about 0.2 larger, while the combined Br populations are correspondingly reduced. These features are consistent with the reduced electronegativity of Br

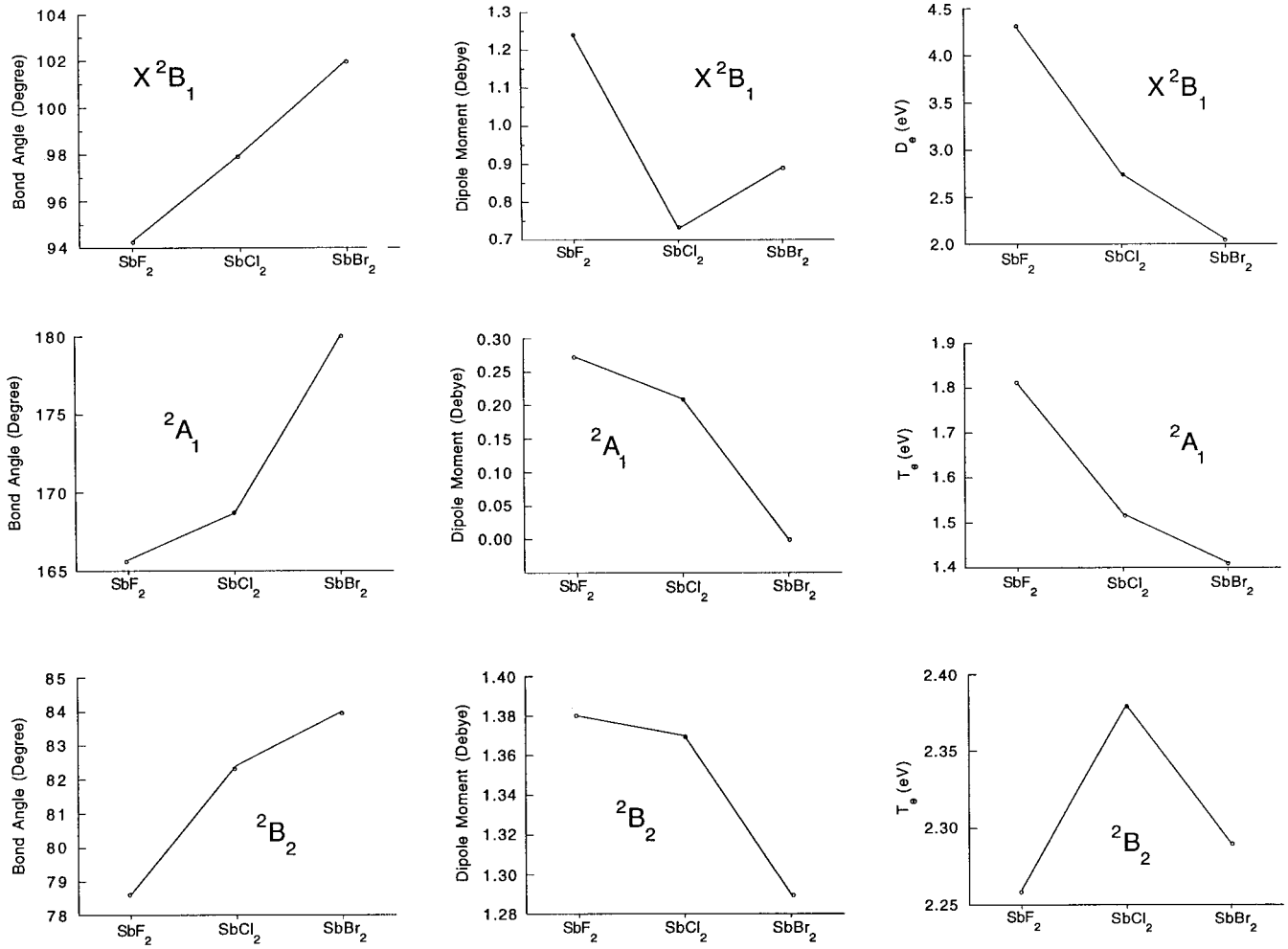

Figure 5. Relative trend in the computed properties of the electronic states of SbF_2, $SbCl_2$, and $SbBr_2$.

so that there is less charge transfer from Sb to Br. The ground state of $SbBr_2$ has an Sb population of 4.19, divided into $5s^{2.00}$-$5p^{2.17}$. The Sb (p) populations in some of the excited states of $SbBr_2$ are considerably higher compared to the X^2B_1 ground state analogous to $SbCl_2$. The leading configurations of the electronic states of the bromine species are quite similar to the chlorine species.

Although there appears to be no spectroscopic studies available at present on $SbBr_2$, there are a few spectroscopic studies on the lighter analogue, namely PBr_2. Thus it appears that comparison of our computed results on $SbBr_2$ with the observed spectroscopic systems of PBr_2 might be of interest.

Bramwell and co-workers[21] have observed a photolysis of PBr_3 by a 193 nm excimer laser, which resulted in several emission systems. A broad structureless system at 527 nm (2.35 eV) was attributed to a fluorescence band of PBr_2 and was assigned to the $\tilde{A}^2A_1 \rightarrow X^2B_1$ transition. The observed long radiative lifetime (21 ± 9 μs) of the electronically excited $\tilde{A}$ state of PBr_2 might suggest that the transition to the ground state from the $\tilde{A}$ state may be weak perhaps due to the symmetry-forbidden nature of this transition. The current authors[25] reassigned the $\tilde{A}$ state of PBr_2 to an excited state of $^2B_2$(I) symmetry, which has a MRSDCI+Q energy separation of 2.78 eV. Although the transition from the $^2B_2$(I) state to the X^2B_1 state is dipole-forbidden, the bending potential energy curve of the $^2B_2$(I) state crosses the $^2A_1$ curve near the minimum of the $^2B_2$(I) curve. Consequently, the $^2B_2$(I) state could couple with the $^2A_1$ state in this region through spin−orbit coupling. Since the spin−orbit coupling is large on the bromine atom, the authors argued that the transition from $^2B_2$(I) to the X^2B_1 ground state could be assisted through the spin−orbit coupling of $^2B_2$(I) and $^2A_1$ states, which would also explain the longer radiative lifetime of the observed $\tilde{A}$ state. The T_e value of the $^2B_2$(I) state of PBr_2 (2.78 eV) was found to be consistent with the experimental value of 2.35 eV for the $\tilde{A}-X$ emission system. As seen from Table 4, the $^2B_2$ state of $SbBr_2$ is computed at 2.38 eV above the X^2B_1 state. Since the energy separation is about 0.4 eV lower than that of PBr_2, we predict the A−X emission transition of $SbBr_2$ to occur at 2 eV. The lifetime of the A state of $SbBr_2$ is expected to be long but shorter than PBr_2 mainly due to larger spin−orbit coupling on both Sb and Br atoms.

Bramwell et al.[21] have also obtained additional emission bands attributed to PBr_2 resulting from the photolysis of PBr_3 using a 248 nm laser excimer. These bands were located at 346 nm (3.58 eV), 366 nm (3.39 eV), 379 nm (3.27 eV), and 407 nm (3.05 eV), which were assigned by the authors[25] on the basis of computed energy separations at the MRSDCI level of 3.55, 3.35, 3.19, and 3.10 eV to the $^2\Pi_g$, $^4\Pi_g$, $^2B_2$(II), and $^4B_1$ states, respectively. As seen from Table 4, the $SbBr_2$ radical also exhibits analogous excited states except that the energy separations differ.

D. $SbBr_2^+$. Figure 4 shows the bending potential energy surfaces of the X^1A_1 and $^3B_1$ and $^1B_1$ electronic states $SbBr_2^+$. The three electronic states of $SbBr_2^+$ are similar to $SbCl_2^+$. Table 4 shows the equilibrium geometries and the energy separations of three electronic states of $SbBr_2^+$. As seen from Table 4, the

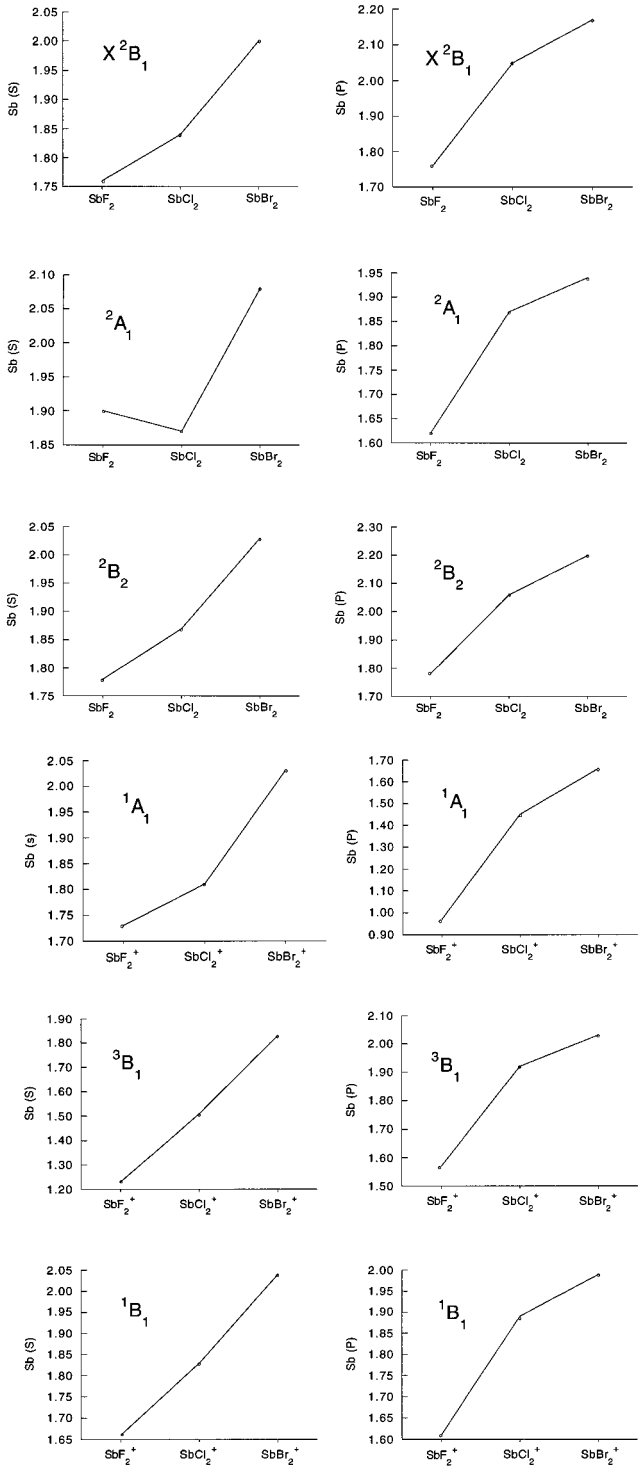

Figure 6. Relative trend in the Mulliken populations of the electronic states of SbF_2, $SbCl_2$, $SbBr_2$, SbF_2^+, $SbCl_2^+$, and $SbBr_2^+$.

ground state of $SbBr_2^+$ is $^1A_1$ with Sb−Br = 2.439 Å and θ_e = 101.8°, compared to the corresponding values of $SbCl_2^+$ (Sb−Cl = 2.279 Å and θ_e = 99.8°). The longer Sb−Br bond lengths and larger Br−Sb−Br bond angle are consistent with the larger sizes of Br relative to Cl atoms. The adiabatic ionization energy of $SbBr_2$ for the process of $SbBr_2(X^2B_1) \rightarrow SbBr_2^+(^1A_1) + e^-$ was computed as 8.08 eV at the highest level of theory, very close to the corresponding adiabatic ionization energy of $SbCl_2^+$ (8.25 eV).

As seen from Table 4, the first excited $^3B_1$ state has a bent equilibrium geometry of r_e(Sb−Br) = 2.471 Å and θ_e = 120.1°,

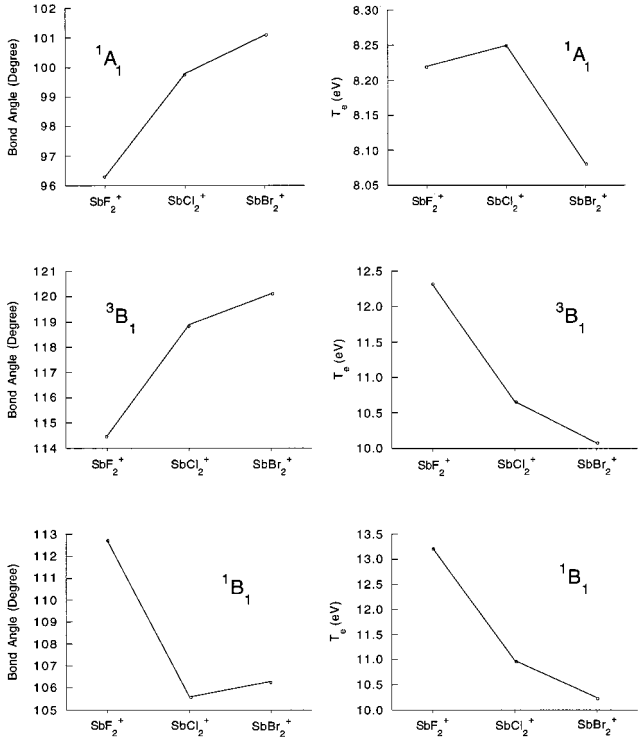

Figure 7. Relative trend in the computed properties of the electronic states of SbF_2^+, $SbCl_2^+$, and $SbBr_2^+$.

while the $^1B_1$ state exhibits an MRSDCI optimized geometry of r_e(Sb−Br) = 2.578 Å and θ_e = 106.3°. The $^3B_1$−X^1A_1 energy separation for $SbBr_2^+$ is 1.99 eV at the MRSDCI+Q level, which is lower than the corresponding value for $SbCl_2^+$. The $^1B_1$−X^1A_1 energy separation for $SbBr_2^+$ is 2.17 eV, which is again smaller than the corresponding value of 2.73 eV for $SbCl_2^+$.

The vibrational frequencies are computed at the UMP2 level as 277.5 cm^{-1} for the A_1 symmetric stretch, 274.0 cm^{-1} for the B_2 asymmetric stretch, and 91.6 cm^{-1} for the A_1 symmetric bending mode for the $^1A_1$ ground state of $SbBr_2^+$. The corresponding B3LYP values are 268.5 cm^{-1} for the A_1 symmetric stretch, 266.7 cm^{-1} for the B_2 asymmetric stretch, and 88.4 cm^{-1} for the A_1 symmetric bending mode for the $^1A_1$ ground state.

The Mulliken populations in Table 5 reveal that for $SbBr_2^+$ in the $^1A_1$ electronic state, the Sb population is 3.67 and the total Br population is 14.33. This suggests that only 52% of the electronic charge is removed from Sb atom upon ionization of $SbBr_2$ in the X^2B_1 state, and thus ionization is almost equally shared between Sb and Br atoms. Again analogous to the chloride species, the Br(p) populations are reduced in the excited states of $SbBr_2^+$. The leading configurations of all the electronic states of $SbBr_2^+$ are the same as those for the corresponding states of $SbCl_2^+$.

E. Comparison of SbX_2 and SbX_2^+ for X = F−Br and with Lighter Halides. Since comparable theoretical studies have been made on SbF_2 and SbF_2^+ and As and P halides,[23−25] it seems to be worthwhile to compare the properties of these species and to establish some periodic trends. It would also be of interest to see the impact of relativistic effects[35] on the properties of heavier halides. The geometries of the ground states of SbX_2 halides are all bent with Sb−X bond distances increasing as one descends from F to Br in the halogen group. The X−Sb−X bond angles increase from 94° to 102° as one moves down the column from F to Br. These trends are shown

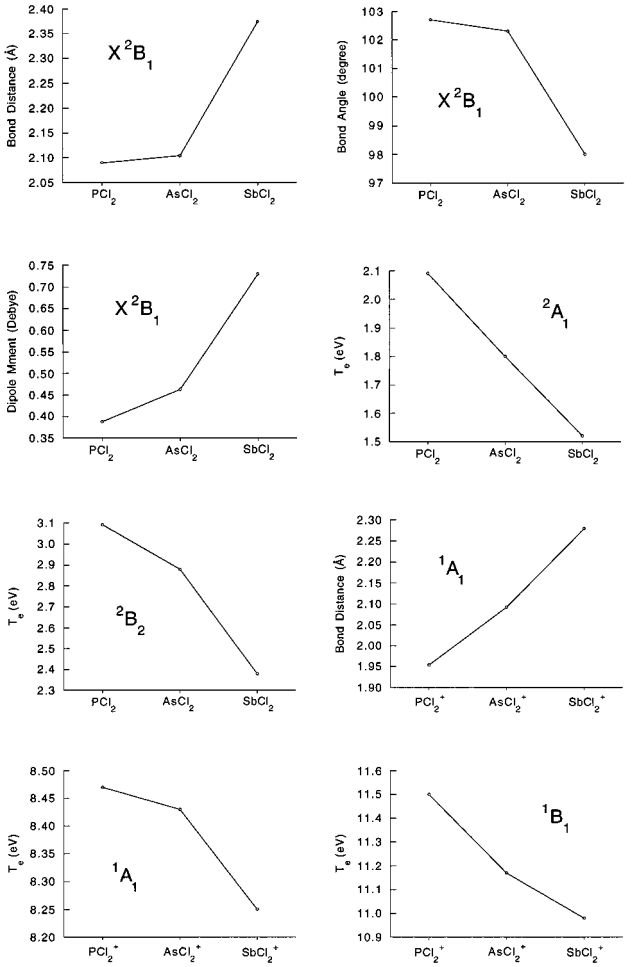

Figure 8. Relative trend in the computed properties of the electronic states of PCl_2, $AsCl_2$, and $SbCl_2$.

in Figure 5 for the geometries and other properties of the various electronic states. As seen from Figure 5, the bond angles increase uniformly. The dipole moment of $SbCl_2$ decreases considerably compared to SbF_2 but the dipole moments of $SbCl_2$ and $SbBr_2$ are quite close (Figure 5). This is consistent with the rapid drop in the electronegativity of Cl compared to F. Although the dipole moments of $SbBr_2$ are slightly larger than those of $SbCl_2$, the μ_e/r_e ratio for $SbCl_2$ is larger than for $SbBr_2$, consistent with the electronegativity trend of Cl and Br. As seen from Figure 5, the dissociation energy of SbF_2 (4.31 eV) is considerably larger than for $SbCl_2$ (2.75 eV) and $SbBr_2$ (2.05 eV). This is fully consistent with the enhanced Sb−F bond strength compared to the Sb−Cl and Sb−Br bond strengths. The compounds formed by the second row elements always differ compared to the lower rows.

The $^2A_1$ and $^2B_2$ excited states of these species can be compared on the basis of their geometries and energy separations. As seen from Figure 5, while the $^2A_1$ states of SbF_2 and $SbCl_2$ exhibit bent minima, we could not find such an obtuse bent minimum for $SbBr_2$, which exhibits only a linear minimum. The bond lengths increase as one moves down the column from F to Br. The energy separation of the $^2A_1$ state relative to the ground state for SbF_2 is substantially larger than for $SbCl_2$ and $SbBr_2$. On the other hand, the $^2B_2$ state exhibits a different trend (Figure 5). The energy separations are comparable except for $SbCl_2$ which is slightly larger. This is primarily attributed to the fact that the halogen orbitals do not change substantially in the $^2B_2$ state, while they change in the $^2A_1$ state. The dipole moments of the three species are quite comparable in this state.

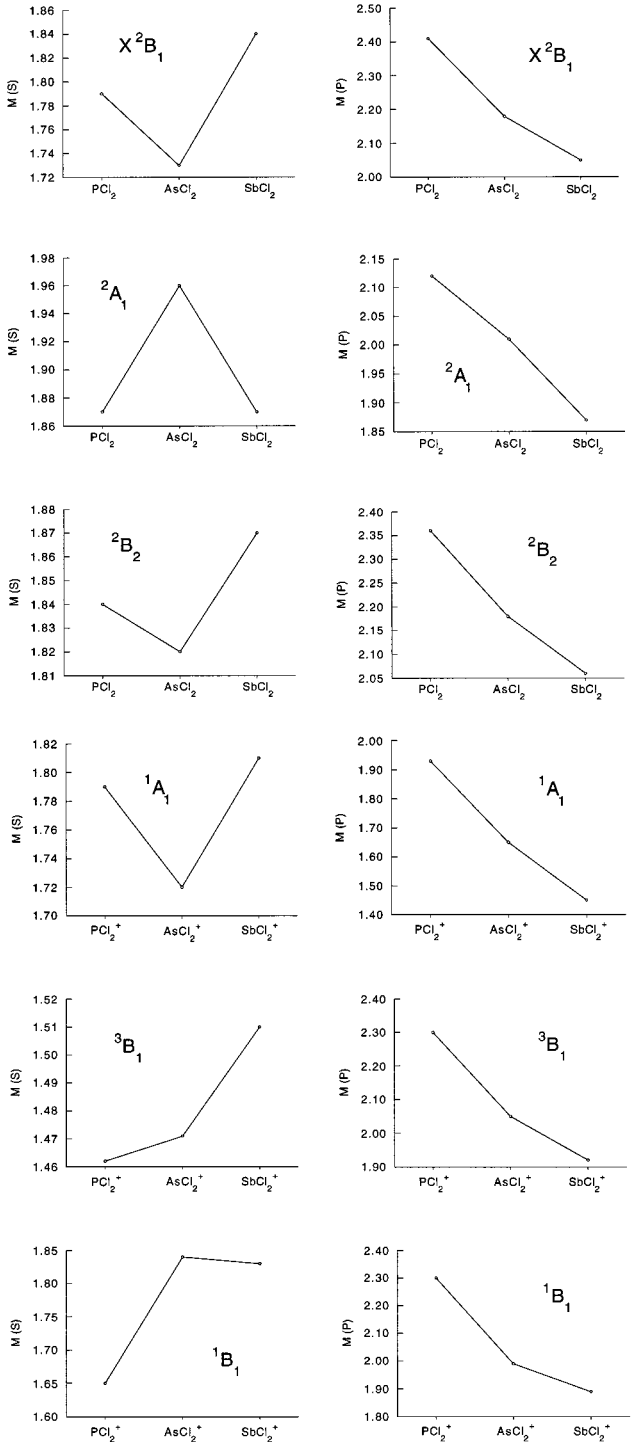

Figure 9. Relative trend in the Mulliken populations of the electronic states of PCl_2, $AsCl_2$, and $SbCl_2$.

The Mulliken populations of the antimony atom in both neutral and positive ions of the three species are compared in Figure 6. The general trend is that the populations differ for the fluoride considerably from the chloride and bromide, but the chloride and bromide species are quite similar. For example, in the ground state it may be seen that the Sb(p) populations are 1.76, 2.05, and 2.17 for SbF_2, $SbCl_2$, and $SbBr_2$. A similar trend is noted in the excited states. For the $^2B_2$ state, we find a uniform increase in the Sb(p) population, as one moves down the group. A striking feature is that the Sb(s) populations for the three low-lying doublet states are very close to 2.0 for $SbBr_2$ indicative of larger relativistic effects[35] in the case of $SbBr_2$ so

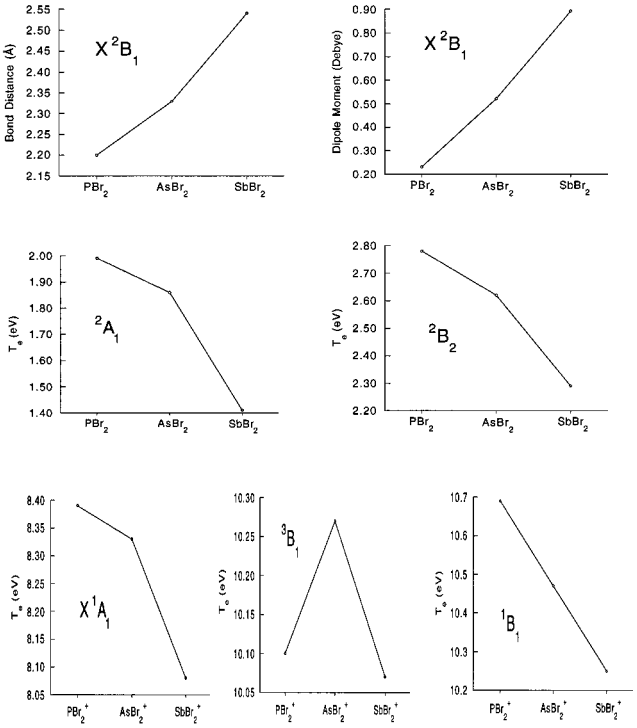

Figure 10. Relative trend in the computed properties of the electronic states of PBr_2, $AsBr_2$, and $SbBr_2$.

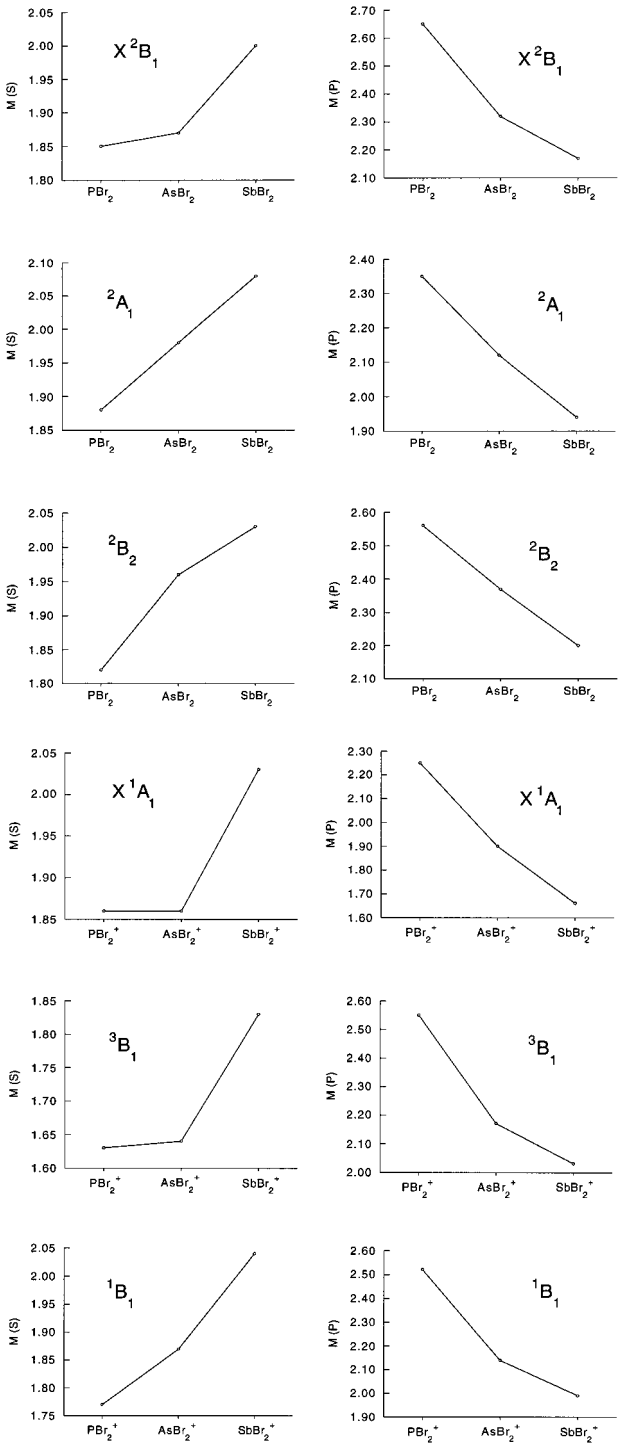

Figure 11. Relative trend in the Mulliken populations of the electronic states of PBr_2, $AsBr_2$, and $SbBr_2$.

that the $5s^2$ shell of Sb becomes relatively inert in the case of $SbBr_2$.

The properties of the positive ions are compared in Figure 7 from which it may be seen that the adiabatic ionization energies of SbF_2 and $SbCl_2$ are quite close but the ionization energy of $SbBr_2$ is slightly lower. This is consistent with the fact that the ionization takes place mostly on Sb for SbF_2^+ and $SbCl_2^+$, while for $SbBr_2^+$, ionization is almost equally shared between Sb and Br atoms. As seen from Figure 7, the bond angles of all the electronic states are nearly the same for the $SbCl_2^+$ and $SbBr_2^+$ ions but differ from SbF_2^+. This is again consistent with the overall trend in many other properties, which reveals fluorides to be different.

The energy separations of the excited states of the positive ions uniformly decrease as one goes down the group, but the drop is substantially larger in moving from F to Cl, as seen in Figure 7. For example, the ionization energy to yield the $^3B_1$ state from the neutral radical is 12.31 eV for SbF_2, while the corresponding values for $SbCl_2$ and $SbBr_2$ are 10.66 and 10.07 eV, respectively, indicating similarity of the chloride and bromide species but difference with the fluorides.

The Mulliken populations of the positive ions are compared in Figure 6. As seen from this trend the Sb populations increase from 2.81 to 3.67 in moving from F to Br, and in particular the Sb(s) population is nearly 2 for $SbBr_2^+$. There is greater increase in moving from F to Cl as compared with Cl to Br, which is fully in accord with the property trends. The Sb(p) populations suffer the largest changes in moving from F to Cl, as seen from Figure 6.

Figure 8 shows the relative trend in the computed properties for PCl_2, $AsCl_2$, and $SbCl_2$ as well as the corresponding positive ions. As seen from Figure 8, the properties of PCl_2 are quite similar to $AsCl_2$ but differ from $SbCl_2$. For example, the r_e values of the $^2B_1$ electronic states of PCl_2 and $AsCl_2$ are 2.092 and 2.104 Å, while the corresponding value for $SbCl_2$ is 2.374 Å. A similar trend is noted in the bond angles and in the energy separations of some excited states. The adiabatic ionization energies of PCl_2 and $AsCl_2$ are quite close, but the corresponding value for $SbCl_2$ is smaller. Relativistic effects seem to become important for Sb compared to As and P.[35]

Figure 9 compares the Mulliken populations of the electronic states of PCl_2 to $SbCl_2$. A general trend is that the Sb(p) populations are substantially smaller for the neutral species. The decrease is larger as one moves from As to Sb compared with P to As. This explains the similarity of PCl_2 and $AsCl_2$ but the difference with $SbCl_2$.

Figure 10 shows the trend in the computed properties of the group V bromides and their positive ions. As seen from Figure 10, analogous to the chlorides, PBr_2 and $AsBr_2$ radicals have

many similarities but the properties of $SbBr_2$ differ. The dipole moments increase as one goes down the group, indicating increased propensity to transfer electronic charge from the group V atom due to decrease in the electronegativity, as one goes down the group. The energy separations of the excited $^2A_1$ and $^2B_2$ electronic states decrease as one goes down the group V.

As seen from Figure 10, in the case of positive ions, the adiabatic ionization energies of PBr_2 and $AsBr_2$ are quite similar but that of $SbBr_2$ is smaller. The excited state energy separations of $SbBr_2^+$ are smaller compared to the lighter analogues. This is partly because ionization is shared between Sb and Br in the case of $SbBr_2^+$, while in case of lighter species ionization takes place predominantly at the group V site.

Figure 11 shows the Mulliken population trends for the group V bromides and their positive ions. The general feature is that the antimony atom has larger s populations and smaller p populations compared with PBr_2^+ and $AsBr_2^+$. The drop in the group V p population is dramatic, especially in moving from P to As for the excited states of PBr_2^+ versus the corresponding states of $AsBr_2^+$. In general, there is decrease in the p population of the group V atom as one goes down the group for all of the states considered in Figure 11. These features are consistent with the other properties of these species and the corresponding chlorides.

IV. Conclusion

In this investigation, we carried out CASSCF computations followed by MRSDCI for several electronic states of $SbCl_2$, $SbCl_2^+$, $SbBr_2$, and $SbBr_2^+$ and SOCI calculations for SbCl and SbBr. The bending potential energy curves of these species were also computed. The dissociation and adiabatic ionization energies have been computed. We have reported the $^3B_1-X^1A_1$ and $^1B_1-X^1A_1$ energy separations of $SbCl_2^+$ and $SbBr_2^+$ in addition to 12 electronic states of $SbCl_2$. Several excited electronic states of $SbCl_2$ and $SbBr_2$ are predicted, none of which is observed at present. However, comparison with the observed spectra of related lighter species reveals that these results are consistent with those spectra. The computed properties of these species were analyzed and compared with the corresponding properties of the lighter species and periodic trends were established. The computed results are in accord with the results obtained for PCl_2, PCl_2^+, $AsCl_2$, $AsCl_2^+$ and the corresponding bromides. We found that the properties of phosphorus and arsenic compounds are similar but those of antimony compounds differ. Likewise, the properties of fluorides of a given group V element were found to differ substantially from the chlorides and bromides of the same element.

Acknowledgment. This research was supported by National Science Foundation. The authors wish to acknowledge the help of Dr. Dingguo Dai in some of the computations.

References and Notes

(1) Haaland, D. M.; Robinson,.M. R.; Koep, G. W.; Thomas, E. V.; Eaton, P. R. *Appl. Spectrosc*. **1992**, *46*, 1575.

(2) Sendra, J. R.; Armelles, G.; Briones, F. *J. Appl. Phys*. **1996.** *79*, 8853.

(3) Vawter, G. A.; Wendt, R. J. *Appl. Phys. Lett*. **1991**, *58*, 289.

(4) Pearton, S. J.; Hobson, W. S.; Baiocchi, F. A. *J. Electrochem. Soc*. **1990**, *137*, 1924.

(5) Jones, R. G.; Singh, N. K.; McConville, C. F. *Surf. Sci*. **1989**, *208*, L34.

(6) Quin, Q. Z.; Lu, P. H.; Zhaung, Z. J.; Zheng, Q. K. *Chem. Phys. Lett*. **1992**, *192*, 265.

(7) Hase, I.; Taira, K.; Kawai, H.; Kaneko, K.; Watanabe, N. *J. Vac. Sci. Technol*. **1989**, *B7*, 618.

(8) Hoekstra, R. J.; Kushner, M. J. *J. Appl. Phys*. **1995**, *77*, 3668.

(9) Edwards, A. J.; Leadbeater, N. E.; Paver, M. A.; Raithly, P. A.; Russel, C. A.; Wright, D. S. *J. Chem. Soc., Dalton Trans*. **1994**, *9*, 1479.

(10) Willey, G. R.; Spry, M. P.; Drew, M. G. B. *Tetrahedron* **1996,** *15*, 4497.

(11) Atwood, D. A.; Cowley, A. H.; Ruiz, J. *Inorg. Chim Acta* **1992**, *198*, 271.

(12) Saito, S.; Endo, Y.; Hirota, E. *J. Chem. Phys*. **1985**, *82*, 2947.

(13) Johnson III, R. D.; Irikura, K. K. *Chem. Phys. Lett*. **1994**, *228*, 273. Zhao, Y.; Setser, D. W. *Chem. Phys. Lett.* **1993**, *210*, 362.

(14) Brum, J. L.; Hudgens, J. W. "Spectroscopic Characterization of AsF2 Radical," private communication.

(15) Yoo, R. K.; Rusciè, B.; Berkowitz, J. *Chem. Phys*. **1992**, *166*, 215.

(16) Brum, J. L.; Hudgens, J. W. *J. Phys. Chem*. **1994**, *98*, 5587. Howe, J. D.; Ashfold, M. N. R.; Hudgebs, J. W.; Johnson, III, R. D. *J. Chem. Phys.* **1994**, *101*, 3549.

(17) Berkowitz, J.; Greene, J. P.; Foropoulos Jr., J.; Neskovic, O. M. *J. Chem. Phys*. **1984**, *81*, 6166.

(18) Wang, O. K. W.; Jones, W. E. *J. Mol. Spectrosc*. **1974**, *49*, 377.

(19) Andrews, L.; Frederick, D. L. *J. Phys. Chem*. **1969**, *73*, 2774.

(20) Bramwell, M. J.; Huges, C.; Jaeger, S. E.; Whitehead, J. C. *Chem. Phys*. **1994**, 183, 127. Bramwell, M. J.; Jaeger, S. E.; Whitehead, J. C. *Chem. Phys*. **1992**, *176*, 547.

(21) Zhao, Y.; Setser, D. W. *J. Phys. Chem.* **1995**, *99*, 12179.

(22) Latifzadeh, L.; Balasubramanian, K. *Chem. Phys. Lett*. **1995**, *241*, 13.

(23) Latifzadeh, L.; Balasubramanian, K. *Chem. Phys. Lett*. **1995**, *237*, 222.

(24) Latifzadeh, L.; Balasubramanian, K. *Chem. Phys. Lett*. **1994**, *228*, 463; **1996**, *258*, 393; **1996**, *262*, 553; J. *Chem. Phys.* **1997**, *106*, 2695.

(25) LaJohn, L. A.; Christiansen, P. A.; Ross, R. D.; Ermler. W. C. *J. Chem. Phys*. **1987**, *87*, 2812.

(26) Hurley, M. M.; Pacios, L. F.; Christiansen, P. A.; Atashroo, A.; Ermler, W. C. *J. Chem. Phys*. **1986**, *84*, 6840.

(27) Huzinaga, S.; Andzlem, J.; Ktobukowski, M.; Radzio-Andzlem, E.; Sakai, Y.; Tatewaki, H. *Gaussian Basis Sets Mol. Calculations* **1984**, 23.

(28) Balasubramanian, K. *Chem. Phys. Lett.* **1986**, *127*, 585.

(29) The major authors of ALCHEMY II are: Liu, B.; Lengsfield, B.; Yoshimine, M.

(30) Balasubramanian, K. *Chem. Phys. Lett*. **1993**, *204*, 601.

(31) Balasubramanian, K. *J. Chem. Phys*. **1989**, *91*, 2443.

(32) Huber, K. P.; Herzberg, G. *Molecular Spectra and Molecular Structure*, *Constants of Diatomic Molecules*; Van Nostrand Reinhold Co.: New York, 1979.

(33) Moore, C. E. *Tables of Atomic Energy Levels*; National Institute of Standards and Technology: Washington, DC, 1971.

(34) Balasubramanian, K. *Relativistic Effects in Chemistry. Part A: Theory & Techniques;* Wiley-Interscience: New York, 1997; 301 p; *Relativistic Effects in Chemistry. Part B: Applications to Clusters & Molecules;* Wiley-Interscience: New York, 1997; 521 p.

(35) Van Huis, T. J.; Yamaguchi, Y.; Sherrill, C. D.; Schaefer III, H. F. *J. Phys. Chem. A* **1997**, *101*, 6955.

(36) Balasubramanian, K. *Chem. Phys. Lett*. **1993**, *204*, 601.

(37) Stephens, J. C..; Yamaguchi, Y.; Sherrill, C. D.; Schaefer III, H. F. *J. Phys. Chem. A*, in press.

(38) Cai, Z. L. *J. Comput. Chem.* **1994**, *15*, 346.

(39) Gustev, G. L. *Chem. Phys.* **1994**, *179*, 325.

(40) Balasubramanian, K. *J. Chem. Phys.*, **1989,** *91*, 2443; **1988,** *89*, 5731.

(41) Boustani, I.; Rai, S. N.; Libermann, H. P.; Alekseyev, A.; Hirsch, G.; Buenker, R. *J. Chem. Phys. Lett.* **1993**, *177*, 45.

(42) Das, K. K.; Alekseyev, A.; Libermann, H. P.; Hirsch, G.; Buenker, R. *J. Chem. Phys.* **1995**, *196*, 395.